Boundary Effects on In-situ Air Permeability Measurements

Shoichiro HAMAMOTO [1), 2)], Ken KAWAMOTO [1), 2)], and Toshiko KOMATSU [1), 2)]
[1)] Soil Mechanics Lab., Department of Civil and Environmental Engineering, Saitama University
[2)] Institute for Environmental Science and Technology, Saitama University

ABSTRACT

In-situ air permeability ($k_{a,insitu}$) measurements give important information on soil-pore structure functions such as air-filled pore connectivity/tortuosity as well as advective soil-gas behaviors in the field. The $k_{a,insitu}$ can be determined by using a shape factor taking account of field geometry effects on one-dimensional air flow. In this study, effects of lateral and bottom boundary conditions on the shape factor (G) and subsequent determination of $k_{a,insitu}$ were investigated by combining finite-element numerical simulations and a model experiment with repacked sand in a container. Results showed that calculated and measured values of G and $k_{a,insitu}$ were highly dependent on the bottom boundary, and especially that a shallow zero-flux bottom boundary caused an underestimation of $k_{a,insitu}$.

KEYWORDS: in-situ air permeability, shape factor, boundary conditions

1. INTRODUCTION

Soil vapor extraction is well known as a remediation technique at polluted soils by Volatile Organic Chemicals (VOCs) such as Tetrachloroethylene and Trichloroethylene (ASTM, 2000). Knowledge of air permeability and its spatial variations at polluted sites are very important for designing and optimizing the system and efficiency of the soil vapor extraction (Toy, 1997; Poulsen et al., 1998, 1999).

Air permeability is a controlling factor for gas advection phenomena due to air pressure gradient in soils. Rapid air permeability measurements at relatively lower cost enable its multipoint measurements at the field sites for a short time (Iversen et al., 2001; Poulsen et al., 2001). The increased use of distributed models in connection with geographical information systems has needed knowledge of the spatial variability of soil physical parameters including air permeability. (Poulsen et al., 2001). In addition, it has been reported that air permeability and other transport parameters such as soil-gas diffusion coefficient, and saturated- and unsaturated hydraulic conductivities are linked (Loll et al., 1999; Iversen et al., 2001; Kamiya et al., 2008; Hamamoto et al., 2011). The data of air permeability also gives important information on connectivity of large pore-networks since air permeability is highly governed by soil-pore size (Osozawa 1998; Hamamoto et al., 2009).

In-situ air permeability can be measured by flowing air at a given inlet air pressure through a ring or pipe inserted into soils (Iversen et al., 2001; Garbesi et al., 1996). In-situ air permeability ($k_{a,insitu}$) is calculated by using a shape factor (G) taking account of field geometry effects on one-dimensional air flow (discussed later). In general, the G is numerically determined based on an air flow model for a homogenous and isotropic medium (Grover, 1955; Boedicker, 1972; Liang et l., 1995; Chief et al., 2008). The existence of a shallow water table or highly-compacted soil layer in the subsurface possibly causes changes of soil-air pressure distribution and inhibits the air flow in soils. Oppositely, the air flow in soils may be enhanced if trenches or holes exist nearby measuring points of the $k_{a,insitu}$. Thus, it is expected that lateral and bottom boundaries in the subsurface highly influence the G values and the calculations of the $k_{a,insitu}$.

In this study, effects of lateral and bottom boundary conditions on the shape factor (G) and subsequent $k_{a,insitu}$ were investigated by combining finite-element numerical simulations and a model experiment with repacked sand in a container.

2. METHOD FOR IN-SITU AIR PERMEABILITY MEASUREMENTS

One-dimensional advective air flux in soils can be described by Darcy's law as,

$$q = -\frac{k_a}{\eta}\left(\frac{dP}{dz}\right) \quad (1)$$

where q is the advective air flux (m s^{-1}), k_a is the air permeability (m^2), η is the viscosity of air (Pa s), and dP/dz is the soil-air pressure gradient (Pa m^{-1}).

It is noted that air conductivity (K_a, m s^{-1}) can be expressed as ($k_a = K_a\eta/\rho g$) where ρ is the density of air (kg m^{-3}) and g is the gravitational acceleration (m s^{-2}).

Air permeability in a laboratory is measured by flowing air at a given inlet pressure through undisturbed or disturbed soil core samples as shown in Fig. 1a (Iversen et al., 2001). Air permeability in a laboratory ($k_{a,\ small}$) can be calculated as,

$$k_{a,small} = \frac{H}{A_s}\frac{\eta Q}{(P_i - P_0)} \quad (2)$$

where H is the sample length (m), A_s is the cross sectional area (m^2), Q is the air flow rate (m^3 s^{-1}), and P_i and P_0 are the air pressure (Pa) at top (inlet) and bottom of the sample, respectively. P_0 is generally assumed as atmospheric pressure, and then the $k_{a,small}$ is calculated by measuring differential air pressure from atmospheric at the inlet and flow rate (Q). As shown in Fig. 1b, in case of in-situ air permeability measurement, the air flow through the soil beyond the end of the air permeameter is not one dimensional. The effects of this divergent flow beyond the outflow end of an inserted soil ring can be addressed by applying a constant unitless factor Λ to Eq. (2) since it is difficult to measure soil-air pressure at the end of soil ring, then $k_{a,insitu}$ can be calculated as (Grover, 1955; Boedicker, 1972; Liang et al., 1995; Chief et al., 2008),

$$k_{a,insitu} = \Lambda\frac{H}{A_s}\frac{\eta Q}{P_i} \quad (3)$$

The Λ can be combined with the height (H) and diameter (D) of the soil ring, to form a dimensionless shape factor (G) as,

$$G = \frac{0.25\pi D}{\Lambda H} \quad (4)$$

By combining Eq. [2.2.3] and Eq. [2.2.4], $k_{a,insitu}$ is can be expressed as,

$$k_{a,insitu} = \frac{\eta Q}{GDP_i} \quad (5)$$

The shape factor (G) is dependent on the diameter (D) and insertion height (H) of the soil ring (Fig. 1b). Predictive models for G presented by Grover (1955), Boedicker (1972), Liang et al. (1995), and Jalbert & Dane et al. (2003) are shown in Table 1. Many predictive models for G are

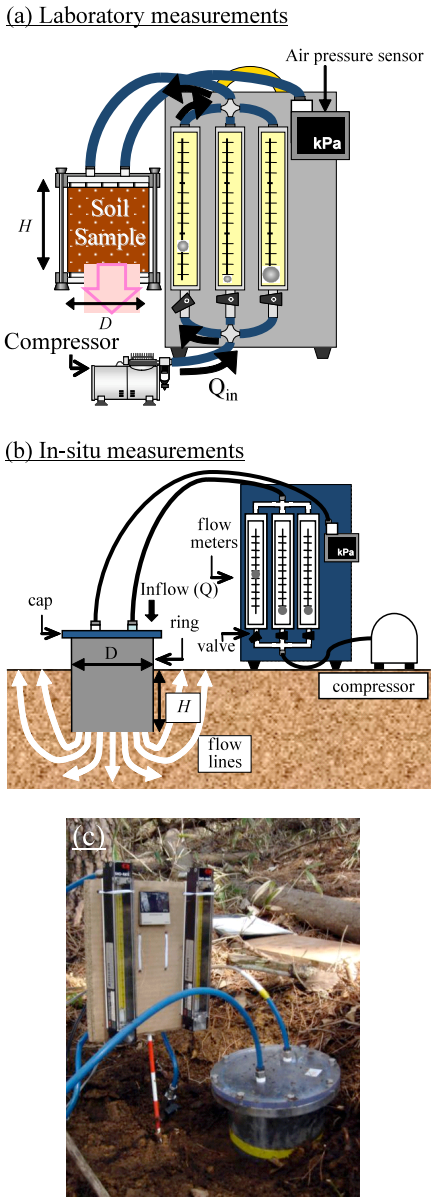

Figure 1 Schematic design of (a) laboratory and (b) in-situ air permeameter. (c) Photo of in-situ air permeameter

expressed as a function of D/H. Grover (1955) experimentally measured a relation between G and D/H by using an air permeameter with a thin-walled cylindrical float. Frevert (1948) used electrolytic model to determine G based on the assumption of identical flow geometry. Boedicker (1972) used an air permeameter similar to that

Table 1 Predictive equations for shape factor G.

Reference	Model Equation
Grover (1955) *	$G = 0.7576(D/H) - 0.1569(D/H)^2 + 0.0140$
Boedicker (1972)	$G = 0.3761(D/H) - 0.0142(D/H)^2 + 0.1075$
Liang et al. (1995)	$G = 0.4862(D/H) - 0.0287(D/H)^2 + 0.1106$
Jalbert & Dane (2003)	$G = (\pi/4 + D/H)(1 + D/H)^{-1}\ln(1 + D/H)$

* Experimental data was multiplied by 0.229 for $D/H < 2.0$ as suggested by Kirkham et al. (1958)

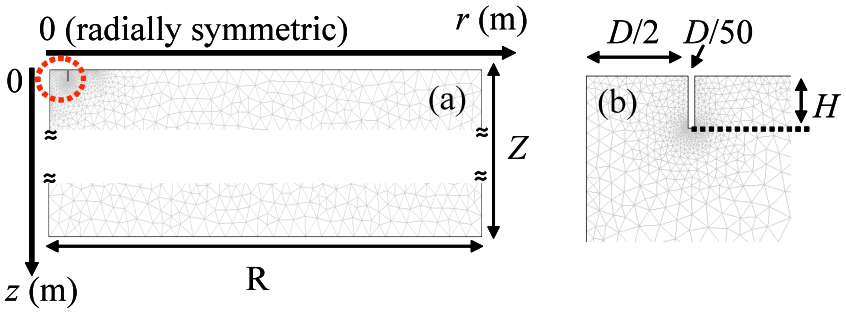

Initial Condition:
$P_e = 0$

Boundary Condition:
$r = 0$, $\partial P_e / \partial r = 0$
$r = R$, $\partial P_e / \partial r = 0$ (Case 1~3)
$P_e = 0$ (Case 2)
$z = 0$ & $(D/2+D/50 < r \le R)$, $P_e = 0$
$z = 0$ & $(0 \le r \le D/2)$, $P_e = P_i$
$z = Z$, $\partial P_e / \partial r = 0$

Figure 2 Finite element mesh for (a) the entire model domain and for (b) the region near the permeameter wall.

proposed by Grover (1955) and suggested predictive G model. Liang et al. (1995) developed a two-dimensional finite-element air flow model for a homogenous and isotropic medium in cylindrical coordinates to estimate the G. More recently, Jalbert and Dane (2003) also developed the same two-dimensional air flow finite-element model but with a larger simulation volume and increased triangular density near the bottom insertion edges. Chief et al. (2008) simulated the air flow in soils using a three-dimensional finite-element method and they validated the shape factor model proposed by Jalber and Dane (2003). They also found that an anisotropy of air permeability in soils highly affects the calculation of $k_{a,insitu}$. Again, these predictive models for G are mainly based on numerical simulations of air flow in homogeneous and isotropic porous media where model domain size is large enough not to affect soil-air pressure distributions by boundary conditions.

3. DETERMINATION OF SHAPE FACTIR

3.1 Governing equations of air flow in soils and numerical simulation model

A transient three-dimensional air flow in soils can be described as (Kirkham, 1946),

$$\nabla^2\left(\frac{k_a}{\eta}P^2\right) = 2\varepsilon\frac{\partial P}{\partial t} \quad (6)$$

where ε is the soil-air content (m^3 m^{-3}). Soil-air-pressure (P) can be defined as,

$$P = P_a + P_e \quad (7)$$

where P_a is the atmospheric pressure (Pa), and P_e is the differential pressure from atmospheric (Pa). At steady state, when P_e is quite lower than P_a ($P_a >> P_e$), Eq. (6) can be expressed as (Kirkahm, 1946),

$$\nabla^2\left(\frac{k_a}{\eta}P_e\right) = 0 \quad (8)$$

In cylindrical coordinate system, Eq. (8) can be written as,

$$\frac{1}{r}\left[\frac{k_a}{\eta}\frac{\partial}{\partial r}\left(r\frac{\partial P_e}{\partial r}\right)\right] + \frac{k_a}{\eta}\frac{\partial^2 P_e}{\partial z^2} = 0 \quad (9)$$

In this study, Eq. (9) was numerically solved by a finite-element method using COMSOL

Table 2 Domain size used for numerical simulations.

		Control* (Case 1)		Effect of lateral boundary (Case 2)		Effect of bottom boundary (Case 3)	
D (m)	D/H	Lateral Domain R (m)	Vertical Domain Z (m)	Lateral Domain R (m)	Vertical Domain Z (m)	Lateral Domain R (m)	Vertical Domain Z (m)
0.15	0.25 0.5	10H	10H	-	-	-	-
	1 2 4 6 8 10	12.5D	15D	1.5D, 2D, 3D, 6D, 9D	12.5D	15D	1.5H, 2H, 3H, 6H, 9H

*domain size after Jalbert & Dane (2003)

Table 3 Properties of the soil, air, and air permeameter.

Property	Variable	Value	Reference
Air permeability	K_a	10^{-11} m^2	Chief et al. (2008)
Air viscosity at 15 °C	μ	1.79 x 10^{-5} Pa s	Chief et al. (2008)
Inlet pressure	P_i	264.4 Pa	Liang et al. (1995)
		1000 Pa	Ball and Schjonning (2002)
Ring diameter	D	0.15 m	
Ring thickness		5.0 x 10^{-3} m (D/50)	

multiphysics ver. 3.4 (Keisoku Engineering System Co., Ltd., Tokyo) where a radially symmetric model was used (Fig. 2). The model domain size and parameter values used in the simulations are presented in Table 2 and 3, respectively.

As shown in Table 2, three different model domain sizes with a different ratio of D/H were considered as follows, i) large domain size following Jalbert and Dane (2003) where soil-air pressure distributions are not affected by boundary conditions (defined as "Control"), ii) variable lateral domain sizes with a constant vertical domain size (Z = 12.5D) (defined as "Case 2"), iii) variable vertical domain sizes with a constant lateral domain size (R = 15D) (defined as "Case 3"). P_e = 0 as an initial condition and zero-flux conditions at both bottom and permeameter wall boundaries were used. In addition, two different inlet air pressures, P_i of 264.4 (Pa) from Chief et al. (2008) and P_i of 1000 (Pa) from Ball and Schjønning (2002) were tested in the simulations. For Case 1 and 3, we used a zero-flux lateral boundary, while for Case 2, P_e = 0 as well as zero-flux condition as a lateral boundary were tested in order to investigate how the existences of opening spaces or shielding materials nearby in-situ air permeameter influence the G values. A predefined triangular mesh size was set with a finer density within and around the air permeameter. The number of elements ranged from 75,000 to 150,000.

3.2 Results of the shape factor

Figure 3a shows calculated G values as a function of D/H. The G values were calculated by Eq. (5) where Q was calculated by integrating the normal component of the calculated boundary flux over the soil surface within the permeameter. The G increased with increasing D/H since higher D/H represents higher soil-air pressure at the end of soil ring. The G values calculated in this study agreed well with predicted G curves proposed by previous studies, especially Jalbert and Dane (2003) (Table 1). Again, Chief et al. (2008) also showed the validity of predictive G model by Jalbert and Dane (2003). Therefore, the predictive G model by Jalbert and Dane (2003) appears promising for calculating $k_{a,insitu}$ for homogenous and isotropic soils when air flow in soils is not inhibited by boundary conditions. Figure 3b shows calculated $k_{a,insitu}$ values as a function of flow rate (Q) by Eq. (5) with different predictive G models including an obtained fitting line from this study at either D/H = 4 or D/H = 10. Lower G values (D/H = 4) caused higher $k_{a,insitu}$ values at a same flow rate as expected by Eq. (5). The calculated $k_{a,insitu}$ values with G values proposed by Boedicker (1972) and Liang et

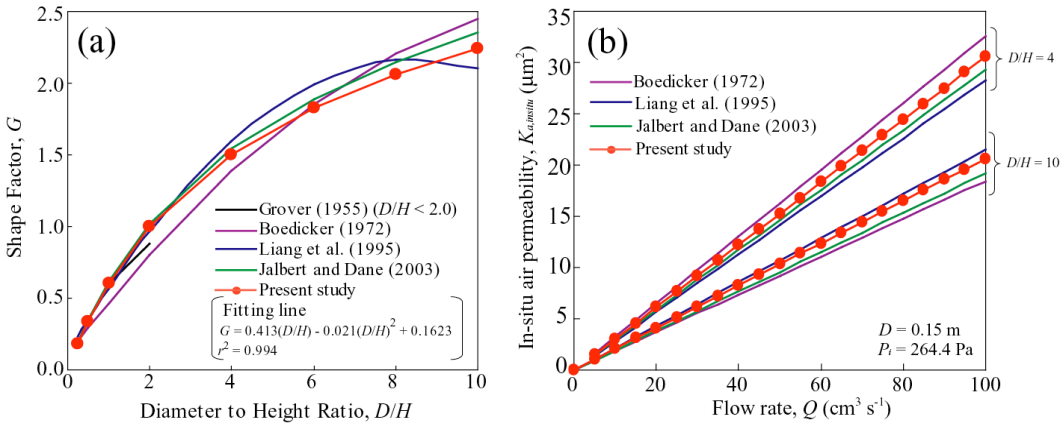

Figure 3 (a) Comparison of shape factor between previous studies and the present study, (b) Calculated in-situ air permeability ($K_{a,\ insitu}$) by shape factor from previous studies and the present study.

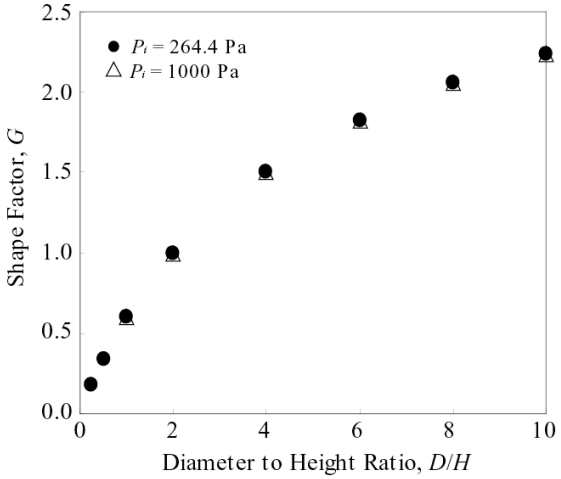

Figure 4 Effect of inlet pressure on shape factor.

al. (1995) models showed upper and lower limits, respectively, and the $k_{a,insitu}$ by using Boedicker (1972) model was around 1.2 times higher than Liang et al. (1995) model at each D/H = 4 and D/H = 10.

3.3 Effects of Boundary Conditions on the Shape Factor

Figure 4 shows the calculated G values as a function of D/H based on the numerical simulations with two different inlet air pressure (P_i = 264.4 or 1000) in the model domain size of Control (Table 2.2.2). As shown in Fig. 4, model predictions by using P_i of 264.4 and P_i of 1000 showed similar G values as a function of D/H, indicating effects of an inlet air pressure on the G were negligible. When a laminar air flow in soils was assumed, air pressure dissipations in the soils are governed only by lateral and bottom conditions in the model domain (Eq. (8)). Therefore, these results confirm the validity of the numerical simulations performed in this study. However, in practice, high inlet air pressure (P_i) than 1000 Pa should be addressed because it causes a turbulent air flow in soils (Ball

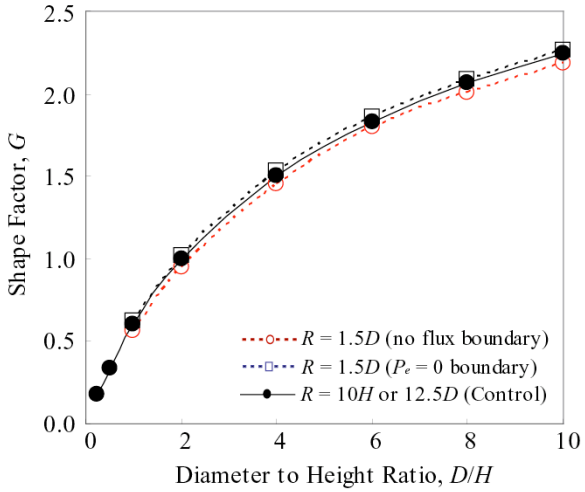

Figure 5 Effect of lateral boundary conditions on shape factor.

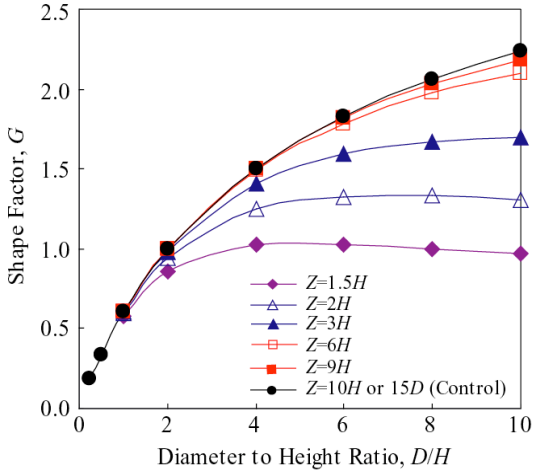

Figure 6 Effect of bottom boundary conditions on shape factor.

and Schjønning, 2002; Bear, 1972; McCarthy and Brown, 1992).

Figure 5 shows effects of lateral boundary conditions on the G. When R is equal to 1.5D and a zero-flux lateral boundary was set, the predicted G values overall D/H showed 4% lower than the G values obtained in the model domain size of Control, indicating that inhibition of air pressure propagation due to the lateral boundary in soils increased air pressure at the end of soil ring. Oppositely, when R is equal to 1.5D and an atmospheric lateral boundary was set, lower air pressure at the end of soil ring increased the G values. The effects of lateral boundary conditions were observed as shown in Fig. 5, but we can conclude that it is not so significant since when the lateral domain size (R) was set as 2.0D, 3.0D, 6.0D, and 9.0D, the predicted G values agreed well with those obtained in the model domain size of Control within 1% of difference.

Figure 6 shows effect of bottom boundary conditions on the G values. The G values rapidly decreased with decreasing vertical domain size (Z), again representing increased air pressure at the end of soil ring by inhibitions of air pressure propagation due to the zero-flux bottom boundary. In addition, the decrease of the G values was more significant at higher D/H because low insertion depth (i.e., high D/H) gave inadequate air pressure dissipation through the inserted soil ring, also enhancing air pressure at the end of soil ring. The effects of a bottom boundary condition on the G is much more significant than those of lateral boundary conditions (Fig. 5), indicating that existences of a shallow water table or highly-compacted layer (impermeable layer) nearby soil surface should be addressed in the $k_{a,insitu}$ measurements.

4. MODEL EXPERIMENTS TO INVESTIGATE EFFECTS OF BOTTOM BOUNDARY CONDITIONS ON $k_{a,insitu}$

4.1 Material and methods

Toyoura sand at air-dry condition was repacked into a container (0.65 x 0.45 x 0.40 m) at a bulk density of 1.51 (Mg m^{-3}) up to soil depth of 0.12 (m) and $k_{a,insitu}$ was measured inside the repacked container as shown in Fig. 7. A soil ring (diameter: 0.15 m) of the air permeameter was inserted at a different insertion depth (H = 0.03, 0.05, 0.08, and 0.10 m) and air was injected from a compressor at a given flow rate (Q) and inlet pressure (P_i) as shown in Fig. 1b. Experimental conditions were presented in Table 4.

The $k_{a,insitu}$ was calculated by measuring a flow rate and an inlet pressure. Two different G values were used in the calculation as follows, 1) the G values predicted by the fitting line from this study (Fig. 3a) where effects of bottom boundary conditions were not considered (i.e., model size of Control), 2) the G values calculated based on numerical simulations using model domain considering actual boundary conditions in the model experiments (i.e., insertion depth, H and vertical domain size, Z) where lateral boundary conditions were set as 12.5 D due to small effects of lateral boundary conditions on the G (Fig. 5 and Fig. 6). Table 3 shows parameter values used in the simulations regarding the properties of the soil, air, and air permeameter. As a reference data, 100 cm^3 core samples (i.d. 5.1 cm, height 5.11 cm) were taken inside the container and air permeability ($k_{a,small}$) was measured. As already described, $k_{a,small}$ was measured by flowing air through the core samples (Fig. 1a) and calculated by measured flow rate and differential pressure across the soil sample (Eq. (2)).

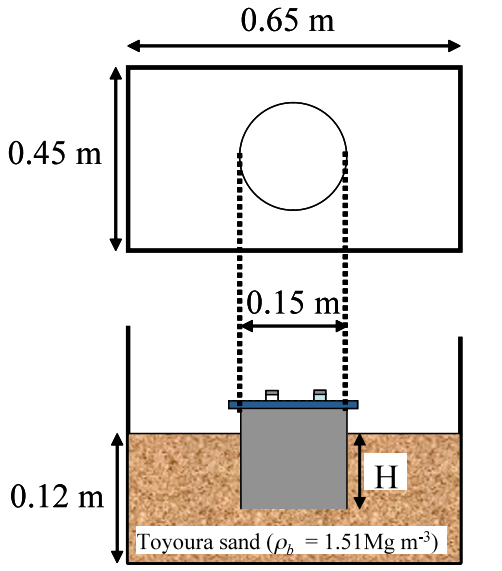

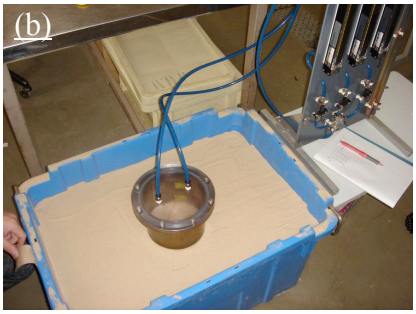

Figure 7 (a) Schematic design and (b) photo of in-situ air permeability measurements for Toyoura sand repacked into a container.

Table 4 Experimental conditions and shape factors for in-situ air permeability measurements for repacked Toyoura sand.

D/*H*	*H* (m)	*Z*/*H*	Shape Factor, *G*	
			Control (fitted line) from Fig. 3a	Considering boundary conditions
5.0	0.03	4.0	1.70	1.60
3.0	0.05	2.4	1.21	1.20
1.9	0.08	1.5	0.89	0.80
1.5	0.10	1.2	0.73	0.54

4.1 Effects of bottom boundary conditions

Fig. 8 shows calculated $k_{a,instu}$ using the G values obtained from two different ways above, and measured $k_{a,small}$ data. The G values used in the calculations of $k_{a,insitu}$ are presented in Table 4. When the G values predicted by the fitting line (Fig. 3a) were used, the calculated $k_{a,insitu}$ decreased with decreasing D/H where the $k_{a,insitu}$ was 30% lower than $k_{a,small}$ at D/H = 1.5. As shown in Fig. 6, the effects of bottom boundary conditions on the G are

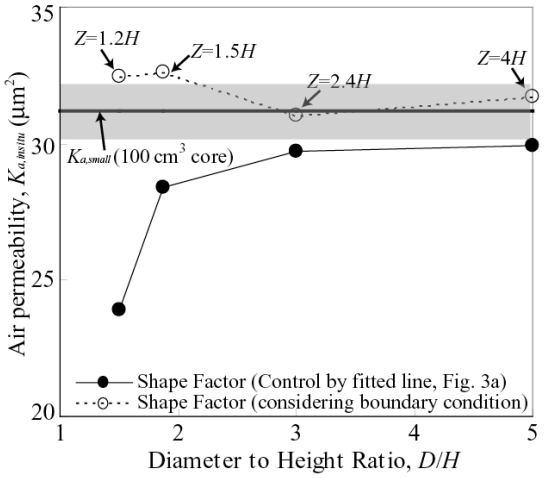

Figure 8 Calculated in-situ air permeability for repacked Toyoura sand. Gray area represents a standard deviation for $K_{a,small}$.

more significant at higher D/H and lower Z/H, giving overestimates of the G. Therefore, at D/H = 1.5, overestimation of G value caused a underestimation of $k_{a,insitu}$ (Table 4 and Fig. 8). When the G values considering bottom boundary conditions was used, calculated $k_{a,insitu}$ showed slightly higher values than $k_{a,small}$ at Z = 1.2H (i.e., D/H = 1.5) and Z = 1.5H (i.e., D/H = 1.9) but it agreed well with the measured $k_{a,small}$ overall insertion depth of H.

5. CONCLUSIONS

The effects of lateral and bottom boundary conditions of the shape factor (G) were investigated by numerical simulations of air flow in soils. When a large model domain (Control) was considered where lateral and bottom boundary conditions do not affect soil-air pressure distribution, obtained G values agreed well with those proposed by Jalbert and Dane (2003). However, numerical simulations using model domain with either variable lateral domain size or variable vertical domain size clearly showed the effects of boundary conditions on the obtained G values. Especially, results showed that calculated G values were highly dependent on the bottom boundary, and that a shallow zero-flux bottom boundary caused a overestimation of G values and subsequent an underestimation of $k_{a,insitu}$. Model tests using repacked Toyoura sand into a container also validated the results of numerical simulations. These findings show that special care must be taken to determine the shape factor with due consideration to the proper boundary conditions. This is especially critical in the case of impermeable layers such as highly-compacted subsurface soil or a shallow groundwater table.

6. REFERENCES

American Society for Testing and Materials (ASTM). (2000) "ASTM E2081-00, Standard guide for risk-based correlative action".

Boedicker, J. J. (1972) "A moving air source probe for measuring air permeability," Ph.D. diss., North Carolina State Univ., Raleigh.

Chief , K., Ferre, T.P.A., and Nijssen, B. (2006) "Field testing of a soil corer air permeameters (SCAP) in desert soils," Vadose Zone J. **V5**, pp.1257-1263.

Chief, K., Ferre, T.P.A., and Hinnell, A.C. (2008) "The effects of anisotropy on in situ air permeability measurements," Vadose Zone J. **V7**, pp. 941-947.

Frevert, R. K. (1948) "Development of a three-dimensional electric analogue with application to field measurement of soil permeability below the water table," Ph.D. diss. Iowa State Univ., Ames.

Garbesi, K., Sextro, R.G., Robinson, A.L., Wooley, J.D. and Owens, J.A. (1996) "Scale dependence of soil permeability to air: Measurement method and field investigation," Water Resour. Res. **V32**, pp. 547-560.

Grover, B. L. (1955) "Simplified air permeameters for soil in place," Soil Sci. Soc. Am. Proc. **V19**, pp. 414-418.

Iversen, B.V., Schjonning, P., Poulsen, T.G., and Moldrup, P., (2001) "In situ, on site and laboratory measurements of soil air permeability: Boundary conditions and measurement scale," Soil Sci., **V166**, pp.97-106.

Jalbert, M., and Dane, J.H. (2003) "A handheld device for intrusive and nonintrusive field measurements of air permeability," Vadose Zone J. **V2**, pp. 611-617.

Kirkham, D. (1946) "Field method for determination of air permeability of soil in its undisturbed state," Soil Sci Soc. Am. Proc. **V11**, pp. 93-99.

Hamamoto, S., P. Moldrup, K. Kawamoto, and T. Komatsu. (2009) "Effect of particle size and soil compaction on gas transport parameters in variably-saturated, sandy soils," Vadose Zone J. **V8**, pp. 986-995.

Hamamoto S., P. Moldrup, K. Kawamoto, and T. Komatsu. (2011) "Two-region Archie's Law Model for Air Permeability and Gas Diffusivity in Variably Saturated Soil," Soil Sci. Soc. Am. J., (in press) .

Kamitani, K., and Inoue, M. (2008) "Functional models to predict air permeability coefficient from water characteristic curve of unsaturated soils," Doboku Gakkai Ronbunshuu C **V64**, pp. 650-661.

Liang, P., Bowers, C.G. Jr., and Bowen, H.D. (1995) "Finite element model to determine the shape factor for soil air permeability measurements," Trans. ASAE, **V38**, pp. 997-1003.

Loll, P., Moldrup, P., Schjonning, P., and Riey, H., (1999) "Predicting saturated hydraulic conductivity from air permeability: Application in stochastic water infiltration modeling," Water Resour. Res., **Vl.35**, pp. 2387-2400.

Osozawa, S. (1998) "A simple method for determining the gas diffusion coefficient in soil and its application to soil diagnosis and analysis of gas movement in soil" (in Japanese with English summary). DSc. Dissertation No. 15 (March 1998) Natl. Inst. of Agro-Environmental Sci., Ibaraki, Japan.

Poulsen, T.G., Moldrup, P., Yamaguchi, T., Schjonning, P, Hansen, J.A., (1999) "Predicting soil-water and soil-air transport properties and their effects on soil-vapor extraction efficiency," Ground Wat. Monit. Remed., **V19**, pp. 61-70.

Poulsen, T. G., Iversen, B.V., Yamaguchi, T., Moldrup, P. and Schjonning P., (2001) "Spatial and temporal dynamics of air permeability in a constructed field," Soil Sci., **V166**, pp. 153-162.

Poulsen, T. G., P. Moldrup, P. Schjønning, J. W. Massmann, and J. A. Hansen (1998) "Gas

permeability and diffusivity in undisturbed soil: SVE implications," J. Environ. Eng. **V12**, pp. 979-986.

Tanner, C. B., and Wengel, R. W. (1957) "An air permeameter for field and laboratory use," Soil Sci. Soc. Am. Proc. **V21**, pp. 663-664.

Toy, M.S. (1997) "Methodology for analyzing soil vacuum data at VOC-contaminated sites," J. Environ. Eng-ASCE, **V123**, pp. 683-690.